N89-12590

MATERIALS SELECTION FOR LONG LIFE IN LEO: A CRITICAL EVALUATION OF ATOMIC OXYGEN TESTING WITH THERMAL ATOM SYSTEMS

S. L. Koontz, J. Kuminecz, L. Leger, and P. Nordine
NASA/Johnson Space Center

Abstract

The use of thermal atom test methods as a materials selection and screening technique for low-Earth orbit (LEO) spacecraft is critically evaluated in this paper. The chemistry and physics of thermal atom environments are compared to the LEO environment. The relative reactivities of a number of materials determined in thermal atom environments are compared to those observed in LEO and in high quality LEO simulations. Reaction efficiencies (cm^3 $atom^{-1}$) measured in a new type of thermal atom apparatus are one-hundredth to one-thousandth those observed in LEO, and many materials showing nearly identical reactivities in LEO show relative reactivities differing by as much as a factor of 8 in thermal atom systems. A simple phenomenological kinetic model for the reaction of oxygen atoms with organic materials can be used to explain the differences in reactivity in different environments. Certain specific thermal atom test environments can be used as reliable materials screening tools. Using thermal atom methods to predict material lifetime in LEO requires direct calibration of the method against LEO data or high quality simulation data for each material.

Introduction

Materials degradation resulting from atomic oxygen attack is an important long life issue for spacecraft operating in the low Earth orbit (LEO) environment. The cost and limited availability of materials test time in flight or in high quality LEO environment simulators has generated considerable interest in the use of thermal energy (0.04 to 0.1 eV) oxygen atoms for materials testing. Thermal atom methods include oxygen plasma ashing, low pressure flowing discharges, and thermal energy beams. While most of these methods can deliver a useful flux of thermal oxygen atoms to the surface of a material test specimen, several fundamental issues need to be resolved before the results of thermal atom testing can be used to support materials selection and development or to estimate the functional life of spacecraft in the LEO environment.

In this paper a critical evaluation of the various thermal atom test methods is presented. The important differences between the thermal atom test environments and the LEO environment are reviewed as are the ways in which various environmental factors may influence materials reactivity measurements. Finally, materials reactivity measurements in several thermal atom environments are compared with measurements made in LEO or in the high quality LEO simulation at Los Alamos National Laboratory (LANL)[24]. The reactivities of organic materials and graphites are the primary focus of this paper. Only passing attention is given to the reactivities of metals and semiconductors. Many of the materials reactivity measurements were made in a new type of flowing discharge apparatus reported here for the first

time. The new apparatus is designed to permit a reasonably accurate estimate of the thermal atom flux at the surface of a material test specimen so that reaction efficiencies can be measured at thermal energies. Thermal atom reactivition efficiencies of several materials are reported here for the first time. The limitations of the reactivity and reaction efficiency measurements are discussed. The availability of direct measurements of materials reactivities in LEO, the LANL simulation facility, and three different thermal atom environments led naturally to the development of a phenomenological kinetic model for the reaction of oxygen atoms with organic surfaces over the range of energies 0.03 to 5 eV. While still highly speculative, we present the model here to stimulate discussion and further work in the atomic oxygen community. Space limitation prevents any discussion of atomic oxygen damage morphology. Morphology will be treated in detail in future publications.

Background

Spacecraft operating at altitudes between 200 and 900 km are operating in LEO, where the residual atmosphere is composed predominantly of oxygen atoms with comparable concentrations of nitrogen molecules up to 400 km[1,2]. Spacecraft orbiting at these altitudes travel at velocities of 8 to 12 km/sec (depending on eccentricity), so that ambient oxygen atoms strike ram oriented spacecraft surfaces with translational energies of 5 to 8 eV. The atom flux depends on altitude, solar activity, orbital inclination, and time of day[1,2], with about 10^{15} atoms cm^{-2} sec^{-1} being a nominal value for the NASA Space Station. The effects of the oxygen atom ram flux on about 300 different materials have been investigated in three Space Shuttle flight experiments and one satellite recovery, and are summarized in Table I. Detailed treatments of the flight data are found in references 3 through 23. Impact on spacecraft design is discussed in refrences 25, 26, and 27. It has been well-established that oxidation reactions are the mechanistic basis for materials degradation by atomic oxygen in LEO[27]. No significant contribution from ablation or sputtering has been demonstrated at this writing.

In addition to oxygen atoms, surfaces in the LEO environment encounter low energy charged particles (ionospheric plasma), solar ultraviolet and vacuum ultraviolet (UV and VUV). In polar orbit, high energy charged particles will also be encountered[25]. Synergism between oxygen and other environmental factors is expected to influence the reaction efficiencies of materials in some circumstances but has not yet been investigated in a systematic way. Thermal atom test environments differ significantly from the LEO environment is several important respects. The translational energy of the atoms is about 0.04 eV, not 5.0 eV. In many thermal atom environments, molecular oxygen is more abundent than atomic oxygen and may influence measurements. The relative dose of UV and VUV radiation varies from one type of thermal atom system to another and is not generally well characterized. Finally, some thermal atom environments expose sample materials to a plasma environment much more severe than the ionospheric plasma in LEO and can also heat conductive samples by radio frequency induction. The thermal atom environments investigated in this work are compared, in a general way, with the LEO environment in Table II. The radio frequency (RF) plasma asher and the flowing afterglow are discussed at greater length in the next two sections.

The RF Plasma Asher Environment

The RF plasma asher can be operated over a fairly wide range of pressures and RF powers, producing a wide range of environments. When operating with pure oxygen as the source gas, atomic oxygen yield can vary from 1 to 60 percent, depending on a number of operating variables. Similarly, charged particle density and temperature as well as ultraviolet (UV) flux and spectra can vary over fairly wide ranges[28-31]. Asher environments share one common factor, however. The sample material is always exposed directly to a plasma and an RF field, unless a faraday cage is used to enclose the sample material[32,33]. The RF field can heat conducting samples, or samples containing conducting components, by induction. Charged particle and UV bombardment of the sample can dramatically change the atomic oxygen reactivity, as shown in the results section below. Charged particle bombardment is a common technique for controlling morphology and reactivity in the fabrication of semiconductor devices[34-36].

The most striking differences between the LEO environment and the asher environment are the kinetic energy of the oxygen atoms, the very large flux of oxygen molecules and UV/VUV photons which also strike the test specimen surface. Atoms in LEO have a translational energy of 5 eV, while those in the asher are between 0.04 and 0.06 eV.

For a dissociation yield of 2 percent at a total pressure of 2 torr the oxygen molecule flux on any surface in the plasma is 1×10^{21} molecules cm^{-2} sec^{-1}, while the atom flux is only 4×10^{19}. By themselves, the oxygen molecules are inert, but they can react with sites created by oxygen atom attack in some materials, as indicated by the formation of organic peroxide radicals from alkyl radicals and oxygen in the gas phase[37] as well as the photochemical weathering of polymers[38]. Ozone, hydroxyl radical, and molecular oxygen in excited states are also potential reactants at the sample surface.

Ultraviolet radiation deserves special mention because low pressure discharges in oxygen are a popular means of generating the 130 nm (9.4 eV) resonance line of atomic oxygen. In LEO the flux of short wavelength (high energy) UV radiation is determined by the solar Lyman Alpha line at 121.6 nm (10.1 eV) with a typical flux of about 4×10^{11} photons cm^{-2} sec^{-1} nm^{-1} in LEO. In discharge lamps and plasma ashers, the flux at the oxygen line can be thousands of times higher, providing more opportunity for photochemistry with these high energy, bond-breaking photons[39,40].

The Flowing Afterglow Environment

The flowing afterglow environment is much easier to define than the plasma asher environment. In the flowing afterglow method, a gas containing oxygen flows through a microwave or RF discharge region where oxygen atoms are produced[37,41]. The gas then flows out of the discharge region and cools to near room temperature before contacting the surface of the test material. The flowing afterglow has a long and venerable history as a device for studying the kinetics of oxygen atom reactions in the gas phase[37,41-43], but has seen only limited use in the study of surface reactions[44,49]. The total pressure of the gas is usually between 0.1 and 2 torr. Pure oxygen or

oxygen diluted in an inert gas such as argon or helium may be used[37,41]. The flowing afterglow environment consists of a gas at or near room temperature and containing ground state oxygen atoms and molecules. Low levels of metastable excited states of molecular and atomic oxygen have been observed in flowing afterglows in some circumstances[41]. The concentration of ions and electrons is negligible[37,41], and it is easy to configure the test specimen so that no electromagnetic radiation from the discharge zone reaches the sample. When using pure oxygen as the operating gas, low levels of water vapor (about 0.3 percent by volume) are added to boost oxygen atom yield.

If the concentration of oxygen atoms and the temperature in the gas near the sample surface can be measured or estimated, the atom flux and kinetic energy at the surface can be calculated from classical kinetic theory[50,51]. The surface flux is simply the atom concentration near the surface multiplied by one-fourth the gas kinetic speed ($F=[O]v/4$), and the kinetic energy distribution can be calculated directly from the Boltzman equation ($E=3kT/2$).

Atoms reaching the surface are lost as a result of reaction with the substrate or recombination to form molecular oxygen. The atom concentration near the surface depends on the relative rates of transport to, and atom loss at, the surface, as well as losses in the gas phase and on other surfaces in the system[52]. It is possible that some test system configurations produce transport limited surface reaction measurements instead of true surface reactivities. An analysis of the transport-reaction process is a vital part of test system design and an important aid in understanding test data.

Oxygen atoms are only one of several species striking the test specimen surface. Molecular oxygen, ozone, and hydroxyl radical are also potential reactants, as in the plasma asher environment. The major differences between the asher and the afterglow rest in the flux of excited species, charged particles, and UV photons at the sample surface, which is much smaller for the afterglow than the asher[28,41].

Experimental

Reaction effeciencies with thermal atoms were measured in two different thermal atom systems. Plasma asher measurements were conducted in an LFE Corporation model LTA-302 low temperature plasma asher, operating at 13.56 MHz. Forward Rf powers ranging from 10 to 100 watts were used with working gas pressures ranging from 0.1 to 2 torr. The test matrix is given in the results section below. The working gas was Liquid Air Corporation analyzed (>99.5 percent pure) avaitor's breathing oxygen (MIL-0-27210 E), containing 12 ppm total hydrocarbon and less than 4 ppm water vapor. Except for highly oriented polycrystalline graphite (HOPG) and pyrolytic graphite, all test samples were 2.54 cm diameter disks of film material. Test specimens were exposed to the plasma environment in a pyrex glass sample holder which positioned the samples horizontally on the long axis of the plasma chambers (parallel to the axis of the field coil), as shown in figure 1. The samples rested on a pyrex glass plate. A pyrex cover plate having three 2.03 cm diameter holes (one for each sample position) covered the samples and exposed 3.24 cm^2 of the sample material. The cover plate

protected the edges of the sample from attack by the plasma environment. Other investigators have observed enhanced attack at the edges of organic film samples placed in oxygen plasmas[53,54]. Only the center and forward (i.e., torward the chamber door) sample positions were used in this study. No attempt was made to measure the atomic oxygen concentration in the asher for this study, but the molecular oxygen flux is almost certainly much larger than the atomic oxygen flux at any sample surface. Oxygen atom kinetic energy is estimated to be between 0.04 and 0.05 eV (Temperature is uncertain in the nonequilibrium environment of the asher).

The flowing afterglow apparatus is shown in figure 2. A Raytheon PGM-10 microwave power supply operating at 2450 MHz was used with an Evenson-type discharge cavity to generate a discharge in flowing oxygen gas at pressures between 0.2 and 2 torr. The forced air cooled Evenson cavity was placed near the center of a 20-cm long, 1-cm I.D. quartz tube. About 9 cm downstream from the discharge chamber, the inside diameter of the flow system increased to 4.0 cm. A valve for introduction of NO_2 titrant gas was placed 14 cm downstream from the discharge region, and the sidearm-sample-holder assembly was placed 53 cm downstream from the discharge region. A cold trap was maintained at -50°C between the flow system and a rotary vane vacuum pump. Flow system pressure was measured with an MKS baratron capacatence manometer. All glassware was given a final cleaning before use by soaking overnight, first in concentrated nitric acid and then in concentrated hydrochloric acid, with a final rinse in demineralized distilled water.

Avaitor's breathing oxygen from Liquid Air Corporation (>99.5 percent pure, MIL-O-27210 E), containing less than 14 ppm hydrocarbon and 0.5 ppm water vapor, was used as the working gas. The gas flow rate was measured with a calibrated MKS, Inc. mass flow meter. About 10 percent of the total gas flow was diverted through a humidification chamber operated at 1.4 atm and 24°C. As a result, the working gas in the afterglow contained about 0.3 percent water vapor, the value which gave a maximum yield of oxygen atoms as measured by both titration and catalytic probes. Oxygen concentrations of 3 to 4 x 10^{15} atoms/cm^3 were obtained at the titration point, with about 1 x 10^{14} at the sample position. For a working pressure of 2.0 torr, the oxygen flow rate was 93.2 sccm, which corresponds to an average linear velocity of 58 cm/sec and a Renyolds number of 0.0036. In 2 torr of pure oxygen, the half life of atomic oxygen is 0.017 seconds, due almost entirely to recombination. The half life for ozone formation is 0.379 seconds[1,37]. Water vapor should be completely converted to hydroxyl radical near the discharge region, but hydroxyl is lost rapidly by surface reactions on pyrex glass flow systems, so that hydroxyl concentrations at the sample are believed to be negligable[37]. As was the case for the asher, the molecular oxygen flux is much greater than the atomic oxygen flux.

Afterglow oxygen atom concentrations were measured by chemiluminescent titration with NO_2[37,41] and with catalytic recombination probes prepared by coating copper-constant-thermocouples with molten silver[55,58]. The atom kinetic energy is estimated as E = 3kT/2 = 0.039 eV.

Except for the HOPG, all afterglow material samples were run as 1.90 cm diameter disks. When mounted at the sample position at the end of a side-arm in the flowing afterglow system, 1.59 cm^2 of the sample disk is exposed

to atomic oxygen. The remainder of the sample rests on the end of the side-arm tube and is protected from attack. The end of the side-arm tube does not form a vacuum seal with the sample film. A 1.90 cm diameter black anodized aluminum plug presses aginst the back side of the sample and contains a heating element and thermocouple which permit the sample to be heated to a known temperature. The assembly is held in place and a vacuum is maintained with a modified 1.90 cm Cajon tubing union as shown in figure 2.

Kapton HN, FEP teflon, polyethylene, Tedlar, and Mylar samples were all cut from sheets of 2 mil film. The Kapton, FEP teflon, polyethylene, pyrolytic graphite and HOPG were obtained from Bruce Banks at NASA's Lewis Research Center as part of the atomic oxygen effects test program (oxygen effects round-robin). The pyrolytic graphites were cut into a 1.90 cm diameter disks. Tedlar and Mylar film samples were obtained from E. I. duPont de Nemours and Co., Inc. All samples except the HOPG were cleaned by brief rinsing with optical grade solvent, a mixture of 1,1,1, trichloroethylene (75 percent) and ethanol (25 percent) from Analytical Research Laboratories, Monrovia, California. The same sample preparation procedure was used for JSC flight samples for STS-8 and for samples prepared at JSC for test in the LANL high energy beam system 59. After air drying, the samples were stored in a dessicator for at least 48 hours before use. Clean surfaces of HOPG were prepared by applying adhesive tape to the basal plane of the crystal and peeling the top layer, leaving a fresh, clean surface. The HOPG was exposed directly to the afterglow environment at the end of a sidearm, with no attempt to protect the sides of the square sample from reaction. The HOPG samples were squares, about 1 cm on an edge and less than 0.3 cm thick.

Results and Discussion

All the materials examined in the RF asher showed dramatic variation in reaction rates, with changes in RF power and total pressure. The samples in the rear and middle sample positions were weighed at various times during the exposure and the mass loss rate determined by a linear regression analysis of sample mass and time ($M(t) = M_0 - R*t$). The correlation coefficient (Pearson's r) was better than -0.99 for most data and never became greater than -0.98, indicating a good fit to a linear model. Plots of the mass loss data for some materials indicated a brief nonlinear induction period early in the test, but the effect on the data fit was small. A typical data plot is shown in figure 3. Table III shows the values of R/A (units of mg cm^{-2} min^{-1}) and the standard deviation calculated by averaging the rates for both sample positions. Inspection of the data in Table III clearly shows that polyethylene has a much higher mass loss rate than Kapton for all combinations of RF power and total pressure used. Teflon also has a higher mass loss rate than Kapton under most conditions.

Trends in the asher data are more easily discerned if the data is normalized and presented as relative rates. In Table IV the rate is normalized to the Kapton rate for a given set of asher conditions; and in Table V the rates are normalized to the 2 torr, 100 watt condition for each material. Comparison of Tables IV and I shows that the 2 torr, 100 watt condition gives the best agreement with the flight results; but even so, the agreement is qualitative at best. Inspection of Table V shows that Kapton,

polyethylene, and single crystal graphite show similar relative changes in rate with conditions, but that FEP teflon does not, suggesting that FEP teflon is responding to different environmental factors than the other materials, or perhaps reacting by a different mechanism. The reactivity of FEP teflon is greatest at high RF power and low total pressure, suggesting that charged particle or photochemical effects dominate the reaction of fluorocarbons in the asher environment.

Reaction rates obtained in the flowing afterglow were substantially lower than those obtained in the asher. Reaction rates in the flowing afterglow were determined by both single time measurements ($R = (M_1 - M_2)/(t1 - t_2)$) and by measurement of sample mass at several times, followed by linear regression analysis ($M(t) = M_o - R*t$), as for the asher. Correlation coefficients better than -0.99 were obtained in most cases, and data plots show no evidence of nonlinearity. A typical data plot is shown in figure 4. Oxygen atom concentrations were determined by NO_2 titration during each run, and rates were corrected for changes in atom concentration. The average rates, relative rates, and reaction efficiencies are reported in Table VI.

The relative rates of polyethylene and single crystal graphite are nearly the same for the asher and the afterglow. Significantly, the relative rate for FEP teflon was much lower than that observed in the asher, supporting the idea that the teflon reaction in the asher depends on factors other than, or in addition to, atomic oxygen. Tedlar and Mylar also gave relative rates much higher than Kapton in the afterglow. Except for Teflon, these materials showed nearly the same reaction efficiency as Kapton in LEO and in the LANL beam[60].

Reducing the afterglow total pressure and oxygen atom concentration by a factor of 10 gave rates about one-tenth those observed at higher pressure and oxygen concentration. Similar results have been observed by at least one other group, using a plasma asher with an optional faraday cage[61]. With no faraday cage, plasma directly contacts the sample surface, and the relative rates observed are much the same as those reported here. When the samples are placed inside the faraday cage, the plasma cannot come into direct contact with the sample surface. Reactive species diffuse to the sample through openings in the faraday cage, so that the environment is more like that in the afterglow. When the samples are placed inside the faraday cage, the relative rates are comparable to those reported here for the afterglow.

The reaction efficiency of materials with oxygen atoms at thermal energies ($3kT/2 = 0.039$ eV) has been the subject of considerable uncertainty and speculation, though the bulk of the evidence available to date suggests that thermal atoms are much less reactive than hyperthermal atoms[62]. The data shown in Table VI indicate reaction efficiencies one-hundredth to one-thousandth those observed in flight (5 eV) or in the hyperthermal beam (3 eV) at LANL. The thermal atom reaction efficiencies reported here do agree in magnitude with those reported by other workers[62,63] using thermal energy beam systems. More work is needed to improve the precision and accuracy of these reaction efficiencies. Molecular oxygen is the most abundant species striking any surface in the asher or the afterglow, and molecular oxygen should react with organic radical sites produced by oxygen atoms[38]. The effects of molecular oxygen and other species, such as ozone and hydroxyl

radical, are being evaluated as part of an ongoing project at the Materials Branch, Johnson Space Center.

As shown above, the thermal atom test systems reported here produce materials reactivities very different from those observed in LEO or in high quality LEO simulations. Most important, while the relative reactivities of Kapton, polyethylene, Tedlar, and Mylar lie within a few percent of each other in LEO and in the LANL beam, they range over an order of magnitude in the thermal atom systems. If the reaction effeciencies of Kapton, Mylar, Tedlar, and polyethylene are plotted vs the atomic fraction of aliphatic hydrogen (fraction R-H) in the polymer repeat unit, we obtain the results shown in figure 5. The correlation coefficient for reaction efficiency and fraction R-H is 0.98, indicating a strong relationship between chemical structure and reactivity in the afterglow. Relationships between chemical structure and reactivity have also been reported for the asher environment in connection with photoresist stripping[64].

Many of the observations presented above can be rationalized with a simple phenomenological model describing the kinetics of mass loss when a hydrocarbon polymer is attacked by atomic oxygen. The essentials of the model are shown in figure 6. Mass loss occurs sequentially. First, hydrogen atoms are removed, and then more massive atoms, such as carbon. The key idea here is that the hydrogen abstraction rate (k_1) has a strong dependence on atom kinetic energy, and also varies substantially with the type and quantity of C-H bonds in the material. The rate constant for oxygen attack, with mass loss, on the hydrogen depleted surface (k_2) is the same for the materials studied. Fresh surface is exposed at a rate which depends on net mass loss through a proportionality constant k_3. Both reaction rates depend on atom kinetic energy and sample surface temperature, but the hydrogen abstraction rate is limiting at thermal energies, as first proposed by Gramm Arnold[62]. If the Arrhenius activation energies and pre-exponential factors for oxygen atom reaction with gas phase organic compounds can be used as a guide, then an activation energy of about 0.3 eV for hydrogen atom abstraction can be expected with pre-exponential factors which vary by as much as a factor of 10 for different hydrocarbons[42].

If most of the oxygen atom kinetic energy is available for overcoming activation barriers, then as kinetic energy increases from 0.04 eV to 5 eV, the activation barrier for hydrogen atom abstraction will be exceeded and k_1 will become very large. Equation 4 shows that when this happens the mass loss rate will be determined by k_2, and all hydrocarbon materials will have the same or similar mass loss rates as observed in LEO. Table I shows several organics, for example epoxy and polybenzimidazole, for which k_2 is different from that for the four materials considered here, perhaps due to effects of the massive heteroatoms. Polymers containing silicone groups form an inert surface oxide layer which prevents or slows further attack.

Summary and Conclusions

The thermal atom test environments examined as a part of this work produce relative material reactivities and reaction effeciencies markedly different from those produced in LEO or in high quality simulations for several different materials. The LFE corporation LTA-302 plasma asher produces the best (i.e., most like the LEO rates) relative rates with 2 torr of oxygen

and 100 watts of forward power; but even better relative rates are produced when a faraday cage is used to isolate samples from the plasma environment[61]. In either environment, materials which have nearly the same relative rates in LEO vary by a factor of as much as 10, even when the faraday cage is used. These results are not suprising, given the radical differences between the LEO environment and the plasma environment in the asher.

The JSC flowing afterglow produced better relative rates than the LTA-302, and reaction efficiencies between one-hundredth and one-thousandth those observed in LEO or in the LANL beam. Mass loss rates were much lower in the afterglow, as presently configured, due mostly to lower atom flux at the sample surface. Work is in progress to increase the atom flux produced by the afterglow.

The thermal atom test methods examined to date can function as materials screening tools, but only if used cautiously. Accurate life-on-orbit data cannot be produced unless the thermal atom method is calibrated using LEO or high quality simulation data. Care must be taken to avoid environments where photochemical or charged particle processes can swamp or confuse oxygen effects data. The flowing afterglow, the asher-faraday cage combination, and the asher at high oxygen pressure seem the best candidates for development into reliable screening tests at this time. Even so, the environments are still very unlike the LEO environment, and many questions remain to be answered before a reliable screening test can be said to exist. The role of molecular oxygen, if any, and other potential reactants is not clear at this time. Most important, the nature of oxygen atom translational energy effects must be understood as it impacts the chemistry of a wide range of materials.

References

1. Chamberlain, Joseph W.: Theory of Planetary Atmospheres. Academic Press, 1978.

2. Hedin, A. E.; Reber, C.A.; Newton, G.P.; Spencer, N.W.; Brinton, H.C.; Mazer, H.G.; and Pottes, W.E.: A Gobal Thermospheric Model Based on Mass Spectrometer and Incoherent Scatter Data MSIS 2 Composition. J. Geophysical Res., vol. 82, 1977, pp. 2148-2156.

3. Leger, L.J: Oxygen Atom Reaction With Shuttle Materials at Orbital Altitudes. Nasa TM-58246, May 1982.

4. Leger, L.J.; Visentine, J.T.; and Schliesing, J.A.: A Consideration of Atomic Oxygen Interaction with Space Station. AIAA Paper 85-0476, AIAA 23rd Aerospace Sciences Meeting, Reno, Nevada, January 14-17, 1985.

5. Leger, L.J.; et al.: STS Flight 5 LEO Effects Experiment - Background Description and Thin Film Results. AIAA Paper 83-2631, AIAA Shuttle Environment and Operations Meeting, Washington, DC, October-November 1983.

6. Whitaker, A.F.; et al.: LEO Oxygen Effects on Spacecraft Materials. AIAA Paper 83-2632, AIAA Shuttle Environment and Operations Meeting, Washington, DC, October-November 1983.

7. Park, J.J.; et al.: Effects of Atomic Oxygen on Paint and Optical Coatings. AIAA Paper 83-2634, AIAA Shuttle Environment and Operations Meeting, Washington, DC, October-November 1983.

8. Zinner, E.; et al: Erosion of Mylar and Protection by Thin Metal Films. AIAA Paper 83-2636, AIAA Shuttle Environment and Operations Meeting, Washington, DC, October-November 1983.

9. Liang, R.; and Gupta, A.: Mechanistic Studies of Kapton Degradation in Shuttle Environments. AIAA Paper 83-2656, AIAA Shuttle Environment and Operations Meeting, Washington, DC, October-November 1983.

10. Visentine, J.T.; et al: STS-8 Atomic Oxygen Effects Experiment. AIAA Paper 85-0415, AIAA 23rd Aerospace Sciences Meeting, Reno, Nevada, January 14-17, 1985.

11. Whitaker, A.F.: Orbital Atomic Oxygen Effects on Thermal Control and Optical Materials STS-8 Results. AIAA Paper 850416, AIAA 23rd Aerospace Sciences Meeting, Reno, Nevada, January 14-17, 1985.

12. Banks, B.A.; et al.: Ion Beam Sputter-Deposited Thin Film Coatings for Protection of Spacecraft Polymers in Low Earth Orbit. AIAA Paper 85-0420, AIAA 23rd Aerospace Sciences Meeting, Reno, Nevada, January 14-17, 1985.

13. Liang, R.H.; and Gupta, A.: Mechanistic Studies of Interaction of Materials With Energetic Oxygen Atoms in Low Earth Orbit. AIAA Paper 85-0422, AIAA 23rd Aerospace Sciences Meeting, Reno, Nevada, January 14-17, 1985.

14. Gull, T.R.; et al.: Effects of Optical Surfaces at Shuttle Altitudes. AIAA Paper 85-0418, AIAA 23rd Aerospace Sciences Meeting, Reno, Nevada, January 14-17, 1985.

15. Gregory, J.C.; and Peters, P.N.: Measurement of Reaction Rates and Activation Energies of 5 eV Oxygen Atoms With Graphite and Other Solid Surfaces. AIAA Paper 85-01417, AIAA 23rd Aerospace Sciences Meeting, Reno, Nevada, January 14-17, 1985.

16. Smith, K.: Evaluation of Oxygen Interaction with Materials (EOIM) - STS-8 Atomic Oxygen Effects. AIAA Paper 85-7021, AIAA Shuttle Environment and Operations II Conference, Houston, Texas, November 1985.

17. Whitaker, A.F.; et al.: Protective Coatings for Atomic Oxygen Susceptible Spacecraft Materials - STS41-G Result. AIAA Paper 85-7017, AIAA Shuttle Environment and Operations II Conference, Houston, Texas, November 1985.

18. Fromhold, A.T.; et al.: Reaction of Metals in Lower Earth Orbit During Space Shuttle Flight 41-G. AIAA Paper 85-7018, AIAA Shuttle Environment and Operations II Conference, Houston, Texas, November 1985.

19. Zimcik, D.G.; and Maag, C.R.: Results of Apparent Atomic Oxygen Reactions With Spacecraft Materials During Shuttle Flight STS41-G. AIAA Paper 85-7029, AIAA Shuttle Environment and Operations II Conference, Houston, Texas, November 1985.

20. Peters, P.N.; Gregory, J.C.; and Swann, J.T.: Effects on Optical Systems From Interactions With Oxygen Atoms in Low Earth Orbits. Applied Optics, vol. 25, no. 8, April 15, 1986.

21. Visentine, J.T.; and Leger, L.J.: Material Inertactions With the Low Earth Orbital Environment: Accurate Reaction Rate Measurements. AIAA Paper 85-7019, AIAA Shuttle Environment and Operations II Conference, Houston, Texas, November 1983.

22. Proceedings of the SMRM Degradation Study Workshop. The Satellite Servicing Project, Goddard Space Flight Center 408-SMRM-79-0001, May 9-10, 1985.

23. Visentine, J.T.; and Leger, L.J.: Atomic Oxygen Effects Experiments: Current Status and Future Directions, NASA TM, JSC, May 18, 1987.

24. Cross, J.B.; and Cremers, D.A: "High Kinetic Energy (1-10 eV) Laser Sustained Neutral Atom Beam Source." Nuc. Instr. Methods, B13, 658 (1986).

25. Durcanin, J.T.; Chalmers, D.R.; and Visentine, J.T.: The Definition of the Low Earth Orbital Environment and its Effect on Thermal Control Materials. AIAA Paper 87-1599, June 1987.

26. Leger, L; Visentine, J.; and Santos-Mason, G.: Selected Materials Issues Associated with Space Station. SAMPE Quarterly, vol. 18, no. 2, January 1987.

27. Brinza, D.E., ed.: Proceedings of the NASA Workshop on Atomic Oxygen Effects. JPL Publication 87-14, November 10-11, 1986.

28. Jacob, Adir: Plasma Processing - An Art or a Science? Solid State Technology, April 1983.

29. Jacob, Adir: Applications of Low Temperature RF Plasma Etching to Thin-Film Technology. Extended Abstracts, vol. 75, The Electrochemical Society, May 1975.

30. Jacob, Adir: The Versatile Technique of RF Plasma Etching. Solid State Technology, June 1977.

31. Corbin, G.A.; et al: Surface Fluorination of Polymers in a Glow Discharge Plasma; Photochemistry. Macromolecules, vol. 18, 1985, pp. 98-103.

32. Jacob, Adir: The Faraday Cage Patent. United States Patent 4,362,632, Dec. 7, 1982.

33. Photoresist Removal With and Without Equi-etch Chamber Insert. LFE Corporation, Bulletin 8216-TA1, August 1975.

34. Choe, D.HG.; Knapp C.; and Jacob A.: Production RIE -I. Selective Dielectric Etching. Solid State Technology, April 1984.

35. Leahy, Michael F.: Superfine IC geometries. IEEE Spectrum, February 10, 1985, pp. 36-43.

36. Choe, D.HG.; Knapp C.; and Jacob A.: Production RIE -II. Selective Aluminum Alloy Etching. Solid State Technology, March 1985, pp. 165-171.

37. Finlayson-Pitts, B.J.; and Pitts Jr., J.N.: Atmospheric Chemistry: Fundamentals and Experimental Techniques. John Wiley & Sons, 1986.

38. Hawkins, L.W., ed.: Polymer Stabilization. Wiley-Interscience, 1972.

39. Zaidel', A.N.; and Shreider, E.Ya: Vacuum Ultraviolet Spectroscopy. Ann Arbor-Humphrey Science Publishers, 1970.

40. Tanaka, I.; and Lossing, F.P.: Photoionization as a Source of Ions for Mass Spectrometry. The Journal of Chemical Physics, vol. 25, no. 5, November 1956, pp. 1031-1034.

41. Setser, D.W., ed.; Reactive Intermediates in the Gas Phase. Academic Press, 1979.

42. Kerr, J.A.; and Moss, J.S.: CRC Handbook of Bimolecular and Termolecular Gas Reactions. vol. I, CRC Press, Inc., 1981.

43. Herron, J.T.; and Huie, R.E.: Rate Constants for the Reactions of Atomic Oxygen (O^3P) With Organic Compounds in the Gas Phase. J. Phys. Chem. Ref. Data, vol. 2, no. 3, 1973.

44. Paraszczak, J.; Hatzakis, M.; Babich, E.; Shaw, J.; Arthur, E.: Plasma Etching of Polymers for Multilayer Lithography. Microcircuit Engineering, Academic Press, London, 1985.

45. De Jaegere, S.; Willems, M.; and Vinckler, C.: Interactions between Afterglow Products of Microwave-Induced Plasmas and Solids, J. Phys. Chem. 86, 3569-3577, 1982.

46. Dzioba, S.; Este, G.; and Naguib, H.M.: Decapsulation and Photoresist Stripping in Oxygen Microwave Plasma. J. Electrochem. Soc., Solid-State Science and Technology, vol. 129, no. 11, pps. 2537-2541, Nov. 1982.

47. Harteck, P.; and Reeves Jr., R.R: Formation and Reactions of the Excited $O_2(A^3\Sigma^+_u)$ Molecules, Disc. Faraday Soc. 37, 82, 1964.

48. Brennen, W.; and McIntyre, P.: Vibrational Relaxation and Electronic Mutation of Metastable Nitrogen Molecules Generated by Nitrogen Atom Recombination On Colbalt and Nickel. Chemical Physics Letters, vol. 90, no. 6, August 20, pp. 457-460 1982.

49. Chu, Ang-Ling; Reeves, R.R; and Halstead, J.A.: Surface-Catalyzed Formation of Electronically Excited Nitrogen Dioxide and Oxygen. J. Phys. Chem., vol. 90, no. 3, pp. 466-67, 1986.

50. Eggers Jr., D.F.; Gregory, N.W.; Halsey Jr., G.D.; and Rabinovitch, B.S.: Physical Chemistry. John Wiley and Sons, Inc., New York, London, Sydney, 1964.

51. Eyring, H., ed.: Physical Chemistry: An Advanced Treatise. Volume II, Statistical Mechanics, Academic Press, New York, London, 1967.

52. Krongelb, S.; and Strandberg, M.W.P.: Use of Paramagnetic-Resonance Techniques in the Study of Atomic Oxygen Recombinations. J. Chem. Physics, vol. 31, no. 5, pp. 1196-1210 November 1959.

53. Colony, J.A.; and Sanford, E.L.: Mechanisms of Polymer Degration Using an Oxygen Plasma Generator. NASA TM-100681, September 1987.

54. Demonet, C.M.; and Milnes, M.V.: Low Earth Orbit (LEO) Atomic Oxygen Effects Simulation with a Low Temperature Asher. NASA TR IRD 85-001, Rockwell International Space Transportation Systems Division, September 1985.

55. Linnett, J.W.; and Marsden, D.G.H.: Reactions of Oxygen Atoms. Proc. Roy. Soc, A234, 489, 504, 1956.

56. Greaves, J.C.; and Linnett, J.W.: Reactions of Oxygen Atoms. Trans. Faraday Soc., 54, 1323, 1958.

57. Greaves, J.C.; and Linnett, J.W.: Reactions of Oxygen Atoms. Trans. Faraday Soc., 55, 1338, 1959.

58. Marsden, D.G.H.; and Linnett, J.W.: Reactions of Oxygen Atoms. 5th Combustion Symposium, Reinhold, pp. 685, 1955.

59. Evaluation of Oxygen Interaction with Materials-III Experiment: Procedures for Assembly of Disk Sample Specimens Into Passive Sample Carrier. NASA JSC-22054, Materials Branch, Structures and Mechanics Division, LBJ Space Center, February 1986.

60. Cross, J.: Atomic Oxygen Exposure (1.5×10^{17} atoms/(cm^2 sec) at 3eV in neon carrier gas). Samples Prepared and Analyzed at Johnson Space Center. Nuc. Instr. Methods, B13, 658 (1986).

61. Smith, L.A.; and Ian, E.: Unpublished data. Materials and Process Branch, Engineering Division, McDonnel Douglas Astronautics Company, Huntington Beach, California.

62. Arnold, G.S; Peplinski, D.R.; and Cascarano, F.M.: Translational Energy Dependence of the Reaction of Atomic Oxygen with Polyimide Films. J. Spacecraft, vol. 24, no. 5, pp. 454-458 Sept.-Oct. 1987.

63. Zimcik, D.G., Tennyson, R.C.; Kok, L.J.; and Maag, C.R.: The Effect of Low Earth orbit Space Environment on Polymeric Spacecraft Materials. Proceedings of the Third European Symposium on Spacecraft Materials in Space Environment, Noordwijk, The Netherlands, 1985.

64. Golub, M.A.; Lerner, N.R.; and Wydeven, T.: Reactions of Atomic Oxygen [O(^{3}P)] with Polybutadienes and Related Polymers. JPL 87-14, see Ref. 27.

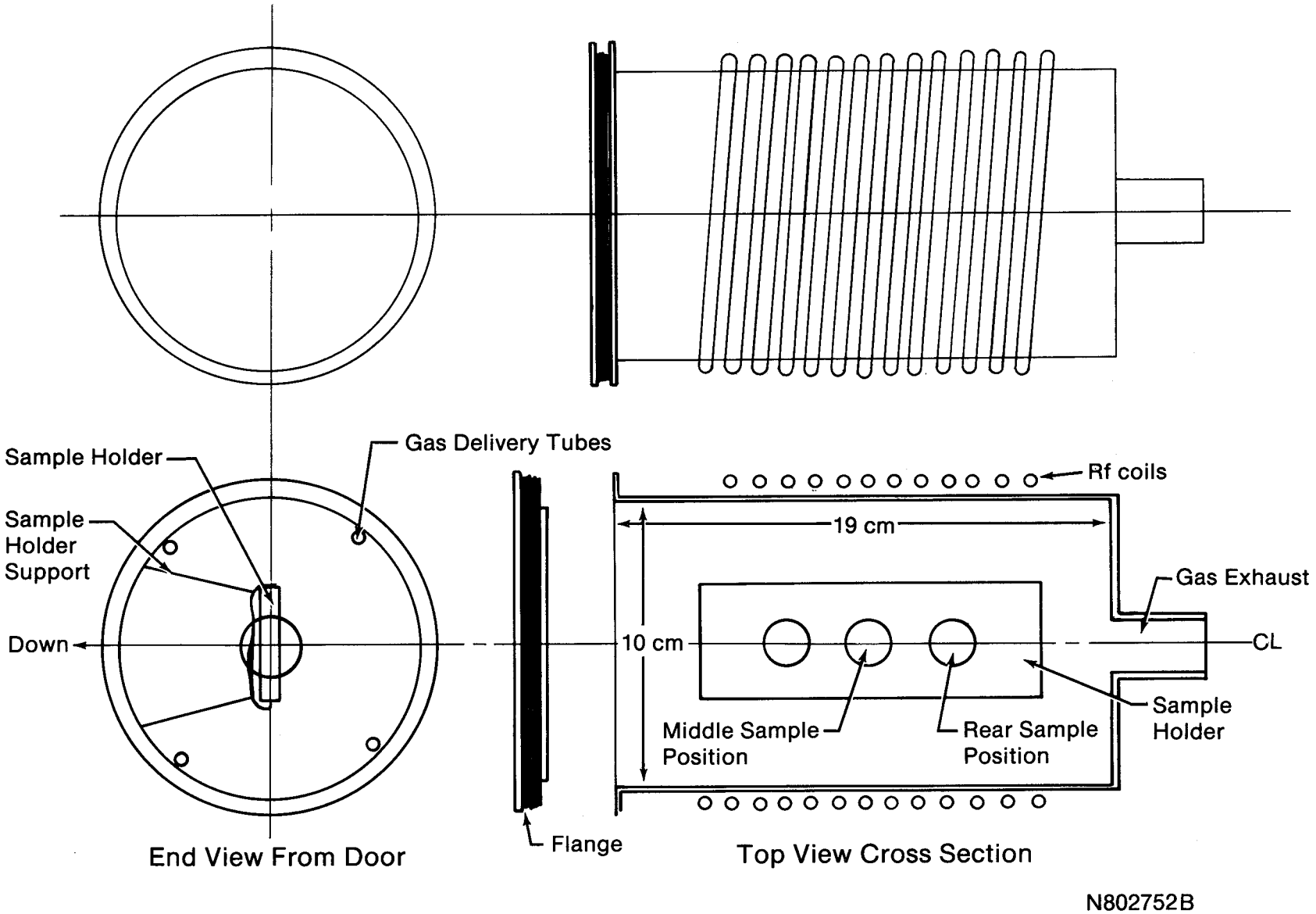

Figure 1.- The plasma asher apparatus configuration.

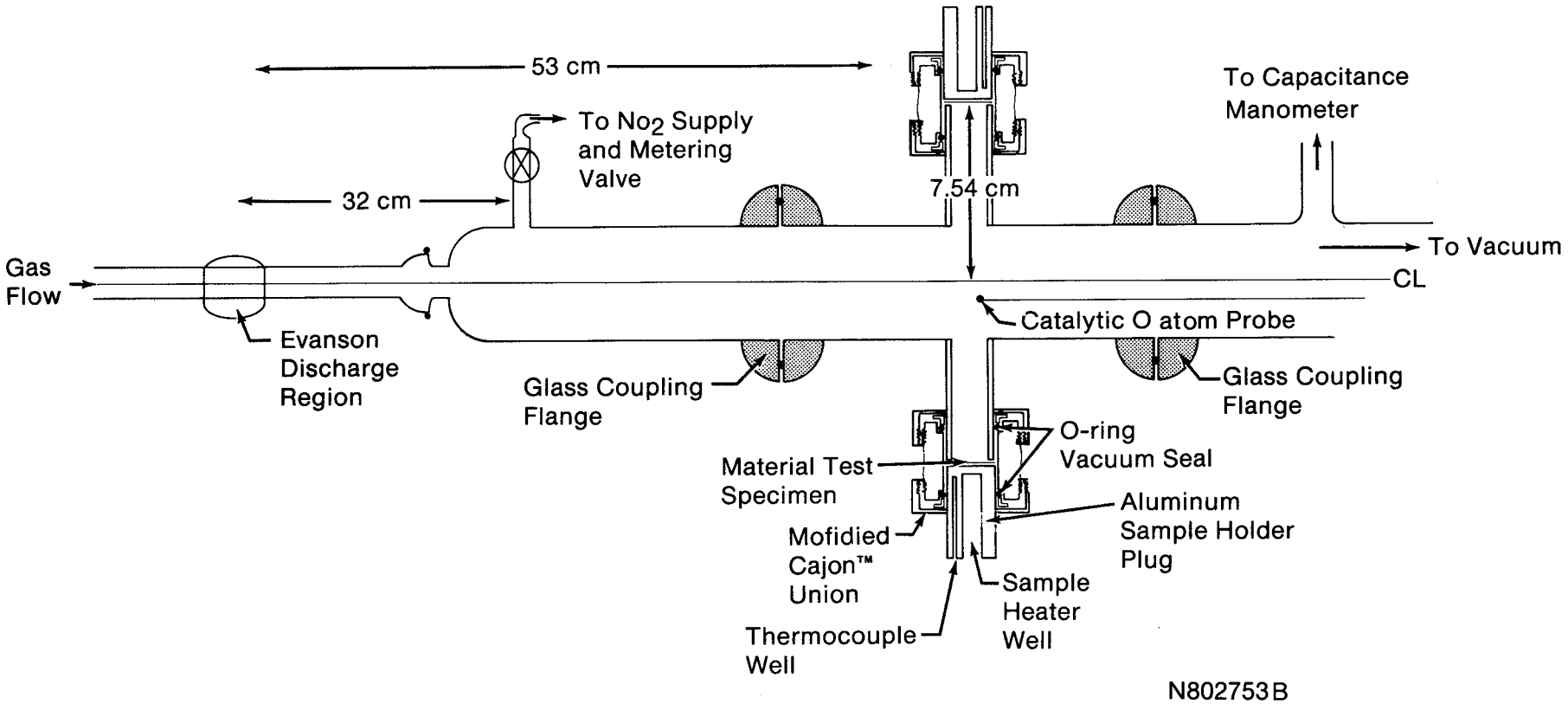

Figure 2.- The following afterglow apparatus configuration.

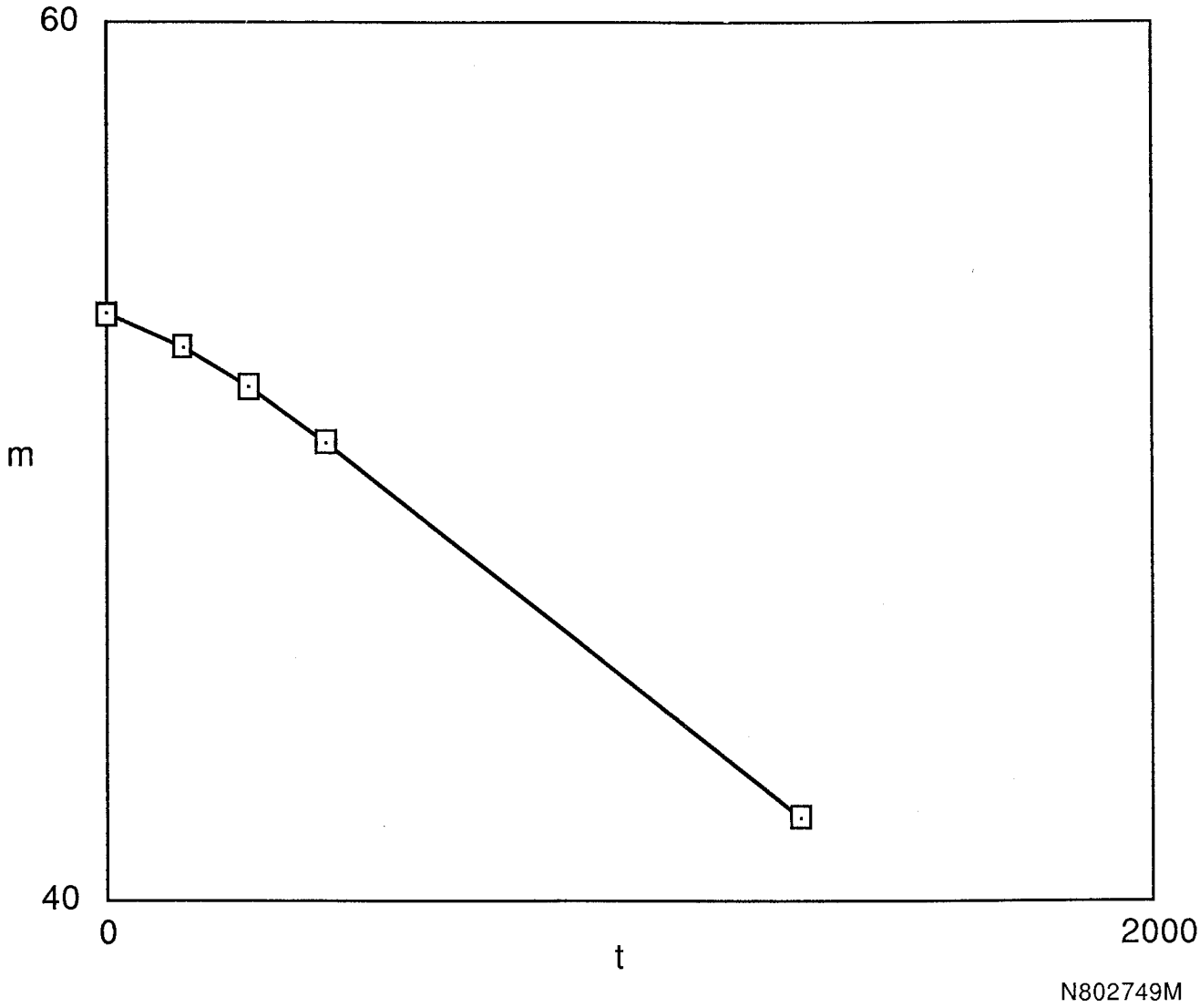

Figure 3.- Sample mass in milligrams vs exposure time for FEP teflon. Typical mass loss data drom exposure of materials to the plasma asher environment. The total pressure was 0.1 torr and the RF power was 10 watts. The small nonlinearity at early exposure times is not typical of all materials and conditions.

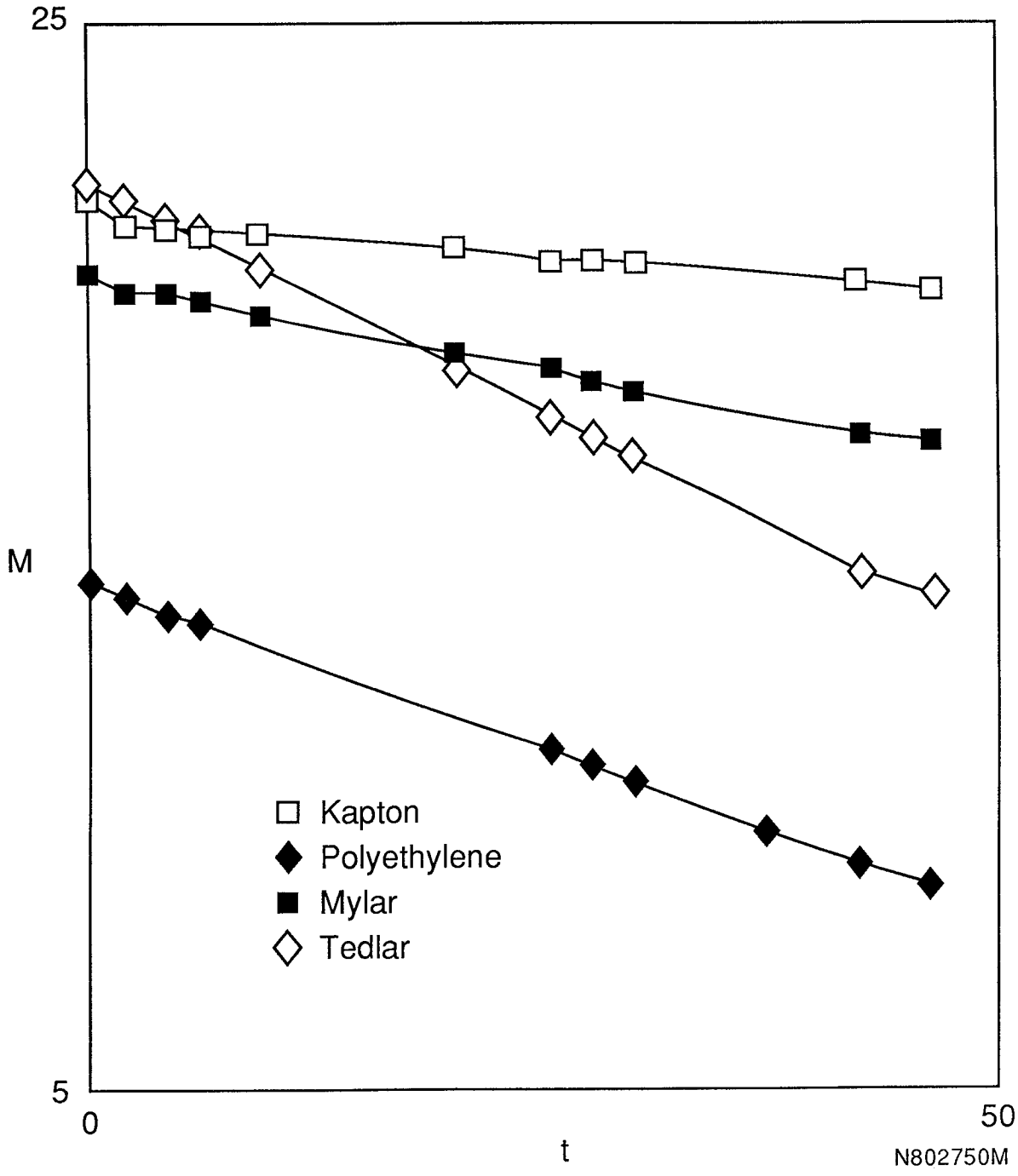

Figure 4.- Sample mass in milligrams vs exposure time hours. Typical mass loss data for exposure of Kapton, Mylar, Tedlar, and polyethylene films to the flowing afterglow thermal atom environment. The oxygen atom flux was 2.1 x $10E^{18}$ atoms cm^{-2} sec^{-1}, and the total pressure was 2 torr.

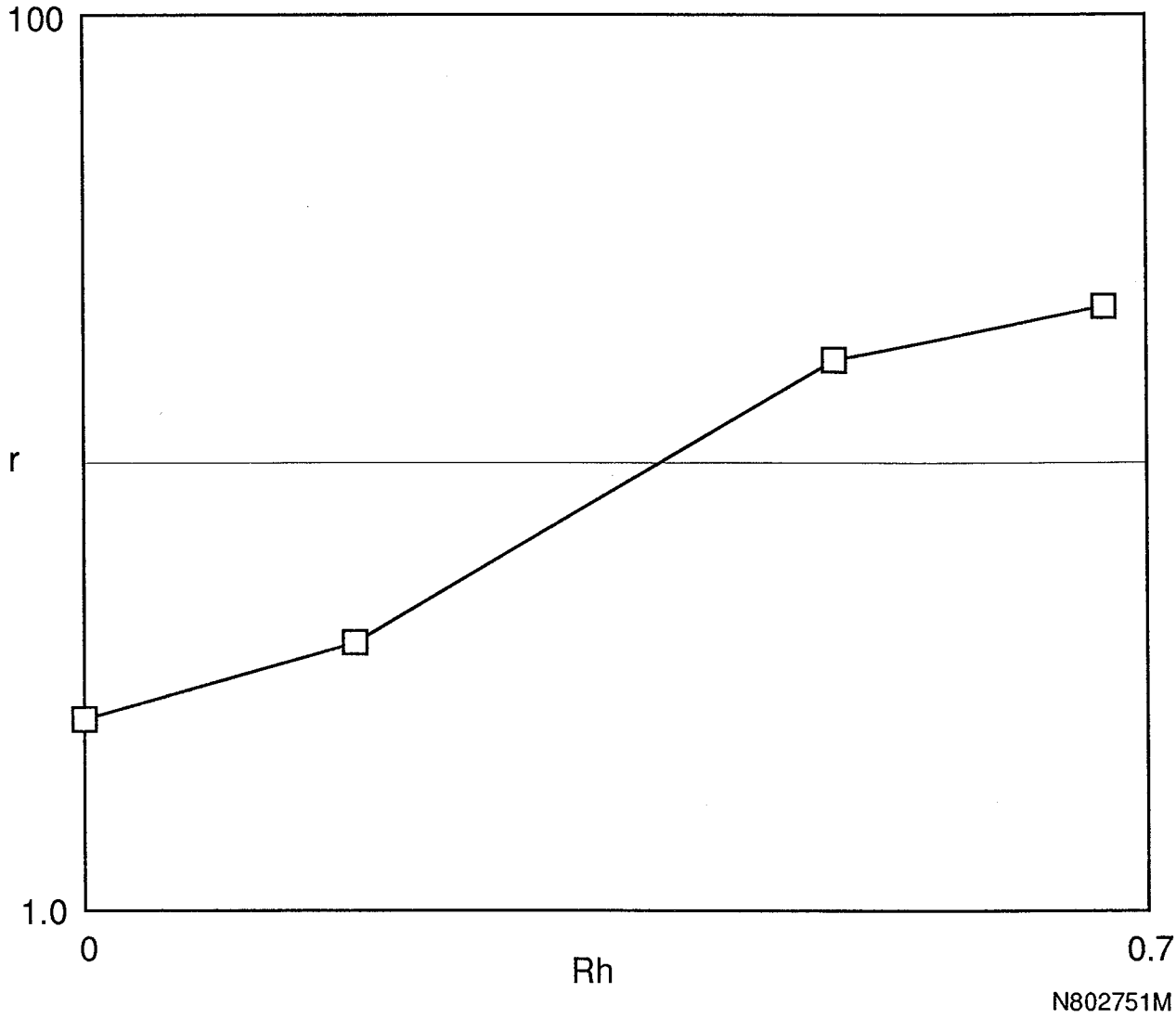

Figure 5.- Reaction effeciency, r is plotted against the aliphatic hydrogen fraction RH in the polymer repeat unit.
RH = # aliphatic hydrogens/total number of atoms. A log plot is used only as a convenience for display of the wide data range. The correlation coefficient for RH and r is 0.969. The correlation coefficient for RH and log(r) is 0.967.

M = sample mass per square centimeter

[R-H] = surface concentration of reactive hydrogen, atoms cm^{-2}

[R-] = surface concentration of dehydrogenated mass loss sites, molecules cm^{-2}

θ = fraction of surface in [R-] state, i.e. fractional dehydrogenation.

At steady state all surface concentrations are constant. The rate constants k_1 and k_2 contain the atomic oxygen flux implicitly; e.g., $k_1 = K_1F$, $k_2 = K_2F$ where F is flux in atoms cm^{-2} min^{-1}.

(1) $d[R\text{-}H]/dt = -k_1(1-\theta) + k_3 dM/dt = 0$

(2) $d[R\text{-}]/dt = -k_2\theta + k_1(1-\theta) = 0$

The chemical reaction rates are related to the mass loss rate.

(3) $dM/dt = -Ak_2\theta - Bk_1(1-\theta) =$ constant (see figures 3 and 4)

A and B are proportionality constants relating mass loss to particular chemical reaction rates.

Combining equations 1,2, and 3 we obtain

(4) $$dM/dt = \frac{1}{k_3/k_2 - 1/Bk_1(1 + Ak_3)}$$

Figure 6.- The essentials of a simple phenomenological model describing the kinetics of mass loss when a hydrocarbon polymer is attacked by atomic oxygen.

TABLE I.- MATERIALS REACTIVITY DATA IN LEO AND LANL BEAM

Material	Rel. Rates*	Reaction Efficiency cm^3/atom	
		LEO (3-23)	LANL (24,60)
Kapton	1	3.0×10^{-24}	2.7×10^{-24}
Polyethylene	0.9	3.7×10^{-24}	2.8×10^{-24}
FEP Teflon	< 0.03	$< 0.05 \times 10^{-24}$	7.7×10^{-25}
Mylar	1	3.4×10^{-24}	
Tedlar	1	3.2×10^{-24}	
Graphite (various forms)	0.7	$0.9 - 1.7 \times 10^{-24}$	10^{-24}
Polybenzimidazole	0.5	1.5×10^{-24}	
Polysulfone	0.8	2.4×10^{-24}	
Siloxane-imide block copolymers (25%/75%)	0.1	0.3×10^{-24}	
Epoxy	0.6	1.7×10^{-24}	
FEP Teflon (Solar Max)	0.6	1×10^{-24}	

*Mass loss rates in LEO normalized to Kapton rate.

TABLE II.- COMPARISON OF ENVIRONMENTS

Environment	O Atom flux, Energy	O_2 molecule flux, Energy	Electron density, Energy	VUV flux, wavelength
LEO	10^{15} atoms cm^{-2} sec^4 5 eV	10^{13} 10 eV	10^5-10^6 e cm^{-3} 0.1 eV	$\sim 4 \times 10^{11}$ 121.6mm
Plasma Asher	10^{19}-10^{20} 0.04-0.06 eV	10^{21} 0.04-0.06 eV	10^9-10^{12} e cm^{-3} 1 to 10 eV	10^{12} to 10^{14} 130mm
Flowing Afterglow	10^{18}-10^{19} 0.04 eV	10^{21} 0.04 eV	$< 10^8$ e cm^{-3} 0.04 eV	0

TABLE III.- MATERIALS REACTIVITY DATA - PLASMA ASHER ENVIRONMENTS

Pressure (torr)	RF (watts)	Kapton*	Polyethylene*	FEP Teflon*	HOPG Graphite*
2	100	1.6 ± 0.3	5.3 ± 0.2	0.27 ± 0.005	0.59 ± 0.006
2	50	0.06 ± 0.01	0.5 ± 0.2	0.18 ± 0.04	-------
0.4	50	0.80 ± 0.2	3.2 ± 0.5	0.49 ± 0.06	-------
0.1	100	0.71 ± 0.2	3.6 ± 0.5	1.1 ± 0.09	0.24 ± 0.06
0.1	10	0.12 ± 0.01	0.45 ± 0.02	0.26 ± 0.02	-------

*Mass loss rates in mg min^{-1} cm^{-2} x 100

TABLE IV.- MASS LOSS RATES RELATIVE TO KAPTON
(mass loss rate divided by Kapton rate)

Pressure (torr)	RF (watts)	Kapton	Polyethylene	FEP Teflon	HOPG Graphite
2	100	1.0	3.4	0.17	0.12
2	50	1.0	8.5	3.0	-------
0.4	50	1.0	4.0	0.6	-------
0.1	100	1.0	5.1	1.6	0.09
0.1	10	1.0	3.6	2.1	-------

TABLE V.- MASS LOSS RATES RELATIVE TO 2 TORR, 100 WATTS CONDITION
(mass loss rate/2 torr, 100 watt rate)

Pressure (torr)	RF (watts)	Kapton	Polyethylene	FEP Teflon	HOPG Graphite
2	100	1.0	1.0	1.0	1.0
2	50	0.04	0.1	0.7	-------
0.4	50	0.5	0.6	1.8	-------
0.1	100	0.4	0.7	4.2	0.4
0.1	10	0.08	0.08	1.0	-------

TABLE VI.- FLOWING AFTERGLOW MATERIALS REACTIVITY DATA

Material	Rel. rate (mass loss)	Mass Loss Rate* (mg cm^{-2} min^{-1})	Reaction Efficiency* (cm^3 per atom)
Kapton	1	$(2.9 \pm 0.3) \times 10^{-4}$	2.6×10^{-27}
Polyeth.	4.1	$(1.2 \pm 0.2) \times 10^{-3}$	2.2×10^{-26}
FEP Teflon	0.07	$(2 \pm 5) \times 10^{-5}$	$< 10^{-28}$
Mylar	2.4	$(7.0 \pm 0.05) \times 10^{-4}$	4.1×10^{-27}
Tedlar	5.9	$(1.7 \pm 0.24) \times 10^{-3}$	1.7×10^{-26}
Graph. (HOPG)	0.2	6×10^{-5}	2×10^{-28}
Graph. (Pyro)	0.07	2×10^{-5}	0.5×10^{-28}

* Average atom flux = 1×10^{20} atoms cm^{-2} min^{-1}